The crystal field and exchange interactions in $Yb_2Ti_2O_7$

2001 J. Phys.: Condens. Matter 13 9301

(http://iopscience.iop.org/0953-8984/13/41/318)

INSTITUTE OF PHYSICS PUBLISHING JOURNAL OF PHYSICS: CONDENSED MATTER

J. Phys.: Condens. Matter **13** (2001) 9301–9310 PII: S0953-8984(01)26843-X

The crystal field and exchange interactions in $Yb_2Ti_2O_7$

J A Hodges[1], P Bonville[1], A Forget[1], M Rams[2], K Królas[2] and G Dhalenne[3]

[1] CEA-Saclay, DRECAM/SPEC, 91191 Gif sur Yvette, France
[2] M Smoluchowski Institute of Physics, Jagellonian University, ulica Remonta 4, 30-059, Kraków, Poland
[3] Laboratoire de Physico-Chimie de l'Etat Solide, Université Paris-Sud, 91405 Orsay, France

Received 6 July 2001, in final form 24 August 2001
Published 28 September 2001
Online at stacks.iop.org/JPhysCM/13/9301

Abstract

In the pyrochlore-structure compounds $R_2Ti_2O_7$, the rare-earth (R) sublattice forms a network of corner-sharing tetrahedra such that the magnetic interactions may be geometrically frustrated. The low-temperature magnetic properties of these compounds are fashioned both by the frustration and by the intrinsic properties of the rare earth, that is, by the degeneracy and anisotropy of the rare-earth crystal-field ground state and by the nature, size and strength of the inter-ionic magnetic coupling. For $Yb_2Ti_2O_7$, we combine ^{170}Yb Mössbauer spectroscopy, ^{172}Yb perturbed angular correlation, magnetization and susceptibility measurements to establish the Yb^{3+} crystal-field level scheme and to show that the crystal-field ground state is a well isolated Kramers doublet having a planar anisotropy. The main contribution to the Yb^{3+}–Yb^{3+} coupling is the exchange interaction which is ferromagnetic. We describe the frustration-related low temperature (<1 K) properties of $Yb_2Ti_2O_7$ in a separate publication.

1. Introduction

The magnetic properties of the rare-earth titanate pyrochlores $R_2Ti_2O_7$ (R^{3+}: $Sm^{3+} \rightarrow Lu^{3+}$) [1] were first studied over 30 years ago [2] and they have attracted renewed attention recently because of the possible influence of magnetic frustration at low temperatures [4–6]. The magnetic frustration has its origin in the geometrical arrangement of the rare-earth sublattice which forms a network of corner-sharing tetrahedra [3]. For each rare earth, the geometrical arrangement of its sublattice remains the same; however, the low-temperature magnetic properties may change markedly from one rare earth to another due to differences in the underlying magnetic properties of the rare earth. These properties comprise the size and anisotropy of the magnetic moments as fashioned by the crystal electric field (CEF) and the

sign, strength and origin (exchange and/or dipole) of the rare-earth–rare-earth coupling. Any detailed examination of the role of magnetic frustration at low temperatures has to be built on the knowledge of the crystal field and the inter-ionic couplings. It is the purpose of this report to present information concerning these two aspects for $Yb_2Ti_2O_7$. As we describe elsewhere [7], this compound does show exotic low-temperature (<1 K) magnetic properties which arise from the frustration.

The CEF properties were obtained from susceptibility and magnetization measurements, ^{170}Yb Mössbauer measurements of the g-values of the ground-state Kramers doublet and ^{172}Yb perturbed angular correlation measurements, up to 1087 K, of the thermal variation of the 4f shell gradient associated with the Yb^{3+} crystal-field levels. The exchange interaction was obtained from susceptibility and magnetization measurements. Combining the different results, we find that in $Yb_2Ti_2O_7$, the Yb^{3+} ion has a ground state which is a well isolated Kramers doublet with a local easy-plane anisotropy and it experiences an exchange interaction which is ferromagnetic.

2. Samples and local site symmetry

Single-phase polycrystalline $Yb_2Ti_2O_7$ was prepared by heating the constituent oxides up to 1400 °C with four intermediate grindings. The single-crystal sample was prepared by the floating-zone technique.

In the pyrochlore lattice, there are 16 equivalent rare-earth sites per unit cell. Each rare-earth site is surrounded by eight oxygens, two lying along a [111] axis at a distance near 0.218 nm and six lying in a buckled plane perpendicular to this [111] axis at a distance near 0.247 nm [9]. The site point symmetry is D_{3d} with the main symmetry axis along one of the [111] directions. For this point symmetry and with Stevens' operator-equivalent formalism, the crystal-electric-field Hamiltonian

$$\mathcal{H} = B_m^n O_m^n \tag{1}$$

involves six non-zero CEF coefficients: B_2^0, B_4^0, B_4^3, B_6^0, B_6^3 and B_6^6. This crystal field lifts the degeneracy of the Yb^{3+}, $4f^{13}$, $^2F_{7/2}$ spin–orbit ground state to leave four Kramers doublets.

3. Experimental results

3.1. ^{170}Yb Mössbauer absorption measurements

To obtain the components of the g-tensor of the Yb^{3+} ground-state Kramers doublet, we use Mössbauer spectroscopy to measure the components of the hyperfine tensor (A) and then we make use of the fact that as J is a good quantum number for Yb^{3+}, the two tensors are proportional. To be able to measure the components of the A-tensor, it is necessary for the Yb^{3+} spin to remain static on the timescale of the Mössbauer measurement ($\sim 10^{-8}$ s). This condition may only be fulfilled when the Yb^{3+} is present at dilute concentration levels. Otherwise, when a Yb^{3+} ion has another Yb^{3+} ion as a nearest cationic neighbour, the ensuing spin–spin interaction leads to a high spin-relaxation rate which wipes out the hyperfine structure.

The measurements were thus made on $(Y_{0.99}Yb_{0.01})_2Ti_2O_7$ (prepared with Yb enriched to a level of 70% in the Mössbauer isotope ^{170}Yb). A source of neutron-irradiated TmB_{12} and a triangular velocity sweep were used. For ^{170}Yb, $I_g = 0$, $I_{ex} = 2$, $E_\gamma = 84$ keV, 1 mm s^{-1} = 68 MHz. Figure 1 shows the data at 4.2 K. The overall absorption pattern is made up of two sub-spectra, one comprising well split components and one comprising a single central line. The well split sub-spectrum ('slow-paramagnetic-relaxation line-shape') is due

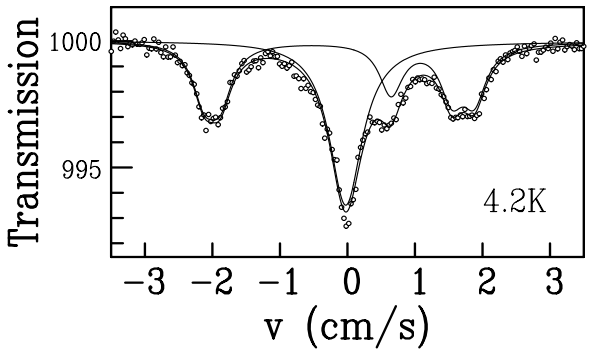

Figure 1. ^{170}Yb Mössbauer absorption in $(Y_{0.99}Yb_{0.01})_2Ti_2O_7$ at 4.2 K. The well split (slow-paramagnetic-relaxation) sub-spectrum provides the principal values of the g-tensor for the Yb^{3+} ground doublet.

to those Yb^{3+} which are magnetically isolated in the sense that they do not have a Yb^{3+} as a nearest rare-earth sublattice neighbour and this sub-spectrum provides the hyperfine tensor. The central single-line sub-spectrum is due to the Yb^{3+} which do have a Yb^{3+} as a nearest neighbour and for which the magnetic hyperfine structure is absent. This latter sub-spectrum has a relative intensity which is stronger than that expected for a purely statistical distribution of the Yb^{3+} over the rare-earth sites, suggesting that the substituted Yb^{3+} undergoes some clustering.

As the rare-earth site has axial symmetry (D_{3d}), the electro-nuclear Hamiltonian is written as

$$\mathcal{H} = \vec{S}' \cdot \mathrm{A} \cdot \vec{I} + \frac{eQV_{zz}}{8}\left[I_z^2 - \frac{I(I+1)}{3}\right] \tag{2}$$

where the local z-axis is along a [111] direction. The first term is the magnetic hyperfine interaction, with A the axially symmetric hyperfine tensor, and the second is the quadrupole interaction with Q the quadrupole moment of the ^{170}Yb $I = 2$ nuclear level and V_{zz} the principal component of the electric field gradient tensor.

For the well split sub-spectrum, the analysis shows that the electronic ground state is a doublet ($S' = 1/2$), $A_z = 463$ MHz, $A_\perp = 1100$ MHz and $eQV_{zz} = -130$ MHz ($V_{zz} = 25$ V Å^{-2}). We then obtain $g_z = 1.79$, $g_\perp = 4.27$ and $\bar{g}$, the average g-value defined as $[(g_z^2 + 2g_\perp^2)/3]^{1/2}$, equal to 3.64. The crystal-field ground state of the Yb^{3+} ion thus has an easy-plane anisotropy with $g_\perp/g_z = 2.4$. We find that the same-size easy-plane anisotropy is present for Yb^{3+} ions diluted into $Lu_2Ti_2O_7$ and it will also be present for Yb^{3+} in $Yb_2Ti_2O_7$ which has essentially the same crystallographic parameters. As will be shown below by our CEF analysis, the small size of the total experimental 4.2 K quadrupole hyperfine interaction is due to the almost complete cancelling of the 4f shell and lattice contributions which have comparable sizes and opposite signs. The single-line sub-spectrum was fitted on the basis of equation (2) using only the quadrupole term. The size of the quadrupole interaction was taken to be the same as that for the well split sub-spectrum.

3.2. Susceptibility and magnetization measurements

The measurements on polycrystalline and single-crystal $Yb_2Ti_2O_7$ were carried out using a commercial SQUID magnetometer. The thermal dependence of the inverse susceptibility for the polycrystalline sample over the range 2.5 to 10 K is shown in figure 2. As will be shown

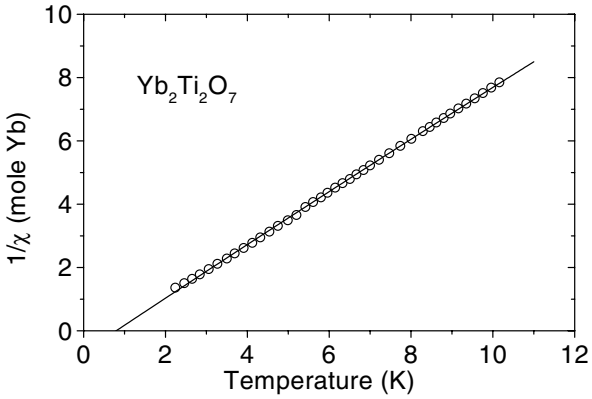

Figure 2. The thermal dependence of the inverse magnetic susceptibility for $Yb_2Ti_2O_7$. The solid line was obtained as described in the text.

by the crystal-field analysis below, the ground Kramers doublet is very well isolated from the excited crystal-field levels. We thus fit the experimental data using the Curie–Weiss expression for a doublet to which is added a Van Vleck term:

$$\chi(T) = \frac{C}{T + \theta_{CW}} + \chi_{VV} \tag{3}$$

where C is the Curie constant ($C = \bar{g}^2\mu_B^2/4$ with $\bar{g}$ defined above), θ_{CW} is the Curie–Weiss temperature and χ_{VV} is the temperature-independent Van Vleck contribution arising from the coupling to the excited crystal-field levels. It was not possible to obtain a well defined value for the Van Vleck contribution directly by fitting the data to equation (3) and it was obtained instead by direct calculation from the crystal-field energies and wave functions derived below. We obtain $C = 1.17(3)$ emu/(mol Yb), $\theta_{CW} = -0.75(10)$ K and $\chi_{VV} = 0.00335$ emu/(mol Yb). The Curie constant is equivalent to an effective moment of $\mu = 3.05(8)\ \mu_B$ and to a ground-doublet average g-value of $\bar{g} = 3.53(9)$. The sign of θ_{CW} corresponds to an interaction which is ferromagnetic in agreement with the literature [2, 8].

The magnetization measurements at 2 K, 5 K and 20 K for the polycrystalline sample are shown in figure 3. The solid lines in figure 3 provide a satisfactory account of the data and were obtained with a model involving an anisotropic Kramers doublet with components g_z and $g_\perp$ and an inter-ionic coupling tensor $\tilde{\lambda}$. When the field H is applied at an angle θ to the local z-axis, the Zeeman splitting of the doublet is $\Delta(H) = g_z\mu_B H\sqrt{P}$, where $P = \cos^2\theta + r^2\sin^2\theta$ and $r = g_\perp/g_z$. At a temperature T, the components of the induced moment along the two principal axes are

$$\mu_z(H, T) = \frac{1}{2}\, g_z\mu_B \frac{\cos\theta}{\sqrt{P}} \tanh\frac{\Delta(H)}{2k_BT} + \chi_{VV(z)} H\cos\theta \tag{4}$$

$$\mu_\perp(H, T) = \frac{1}{2}\, g_z\mu_B \frac{r^2\sin\theta}{\sqrt{P}} \tanh\frac{\Delta(H)}{2k_BT} + \chi_{VV(\perp)} H\sin\theta. \tag{5}$$

The Van Vleck contributions ($\chi_{VV(z)}$ and $\chi_{VV(\perp)}$) are similar and in the following only the average value χ_{VV} is considered. The measured magnetization (the projection of $\vec{\mu}$ along $\vec{H}$) is given by

$$M(H, \theta) = \frac{1}{2} g_z\mu_B\sqrt{P} \tanh\frac{\Delta(H)}{2k_BT} + \chi_{VV} H \tag{6}$$

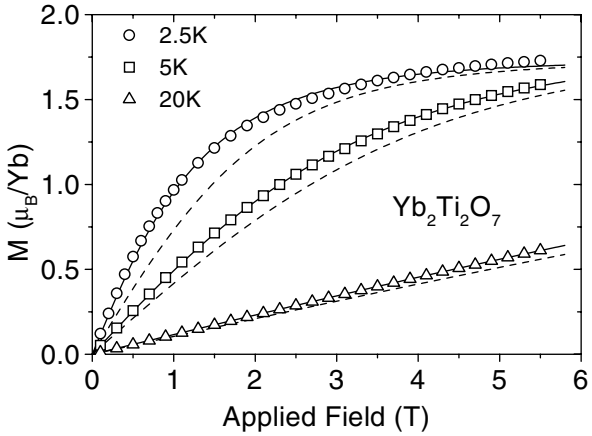

Figure 3. The field dependence of the magnetization for $Yb_2Ti_2O_7$. The solid lines were calculated on the basis of an anisotropic Kramers doublet and a ferromagnetic inter-ionic interaction and the dashed lines represent the variations calculated when this interaction was set to zero.

and the angle-averaged magnetization for a polycrystalline sample is then

$$M(H) = \frac{1}{2}\int_0^{\pi} M(H,\theta)\sin\theta \, \mathrm{d}\theta + \chi_{VV}H. \tag{7}$$

To carry out the self-consistent calculation in the presence of the inter-ionic interactions, $\vec{H}$ must be replaced by $\vec{H} + \tilde{\lambda}\vec{\mu}$; the iterations are carried out until the values of the two components of $\vec{\mu}$ converge.

It is likely that the coupling tensor $\tilde{\lambda}$ is anisotropic. However, we found that the analysis of the magnetization for the polycrystalline sample could not provide any information concerning the size of this anisotropy and, consequently, we assumed that λ is isotropic. This means that the value obtained for λ represents some average of the full inter-ionic interaction. We imposed the anisotropy of the ground-doublet g-tensor so that it was consistent with that provided by the ^{170}Yb Mössbauer measurements and we used the same value for the Van Vleck contribution as for the susceptibility analysis. The fitting procedure (solid lines in figure 3) then involved two adjustable parameters: the size of the average g-value ($\bar{g}$) and the strength and sign of the inter-ionic coupling constant (λ). We obtained $\bar{g} = 3.46(8)$ for each of the three temperatures and $\lambda = 0.31(4)T/\mu_B$ for 2.5 and 5 K (the same value was used for the line shown at 20 K where the dependence on λ was quite weak). The sign of λ corresponds to an interaction which is ferromagnetic and this is in agreement with the sign obtained for θ_{CW}. No acceptable agreement could be obtained between calculation and experiment when the inter-ionic interaction was omitted: the dashed lines in figure 3 illustrate the calculated field dependences of the magnetization obtained using unchanged g-values and assuming that there is no inter-ionic interaction.

We now examine whether the value of λ obtained from the analysis of the magnetization data is consistent with the value of θ_{CW} obtained from the analysis of the susceptibility data. When the size of the inter-ionic interaction is such that it can be treated as a perturbation, i.e. when the product $\lambda\chi \ll 1$ (in the present case, $\lambda\chi \simeq 2 \times 10^{-2}$ at low temperature), the standard molecular field relation linking λ and θ_{CW} for a Kramers doublet can be written as

$$k_B\theta_{CW} = -\frac{1}{4}\bar{g}^2\mu_B^2\lambda f(r,\lambda) \tag{8}$$

where the function $f(r, \lambda)$ is included in order to take into account the anisotropy of the g-tensor. However, from numerical estimates we find that this function, which is exactly equal to unity when the g-tensor is isotropic, also remains close to unity in the present case where $r \simeq 2.4$. For the present purpose, we thus use equation (8) taking $f(r, \lambda) = 1$. Inserting the value of λ obtained from the analysis of the magnetization data into equation (8), we find $\theta_{CW} \simeq -0.64$ K. This matches well with the experimental value obtained directly from the susceptibility data: $\theta_{CW} = -0.75(10)$ K.

The susceptibility and magnetization data analyses are thus consistent with the size of the average g-value of the ground doublet and the sign (ferromagnetic) and strength of the low-temperature inter-ionic coupling constant λ. We mention that we have also obtained another estimate of this constant by examining the thermal dependence of the low-temperature spontaneous Yb^{3+} magnetic moment. The value obtained ($\lambda \sim 0.5T/\mu_B$) is close to that found here.

Although the total inter-ionic Yb^{3+}–Yb^{3+} coupling contains contributions arising from the exchange and the dipole–dipole interactions, because of the small size of the Yb^{3+} magnetic moment, the dipole–dipole coupling will, in fact, only play a very minor role. Scaling the dipole contribution found in $Dy_2Ti_2O_7$ [6] and taking into account the very different sizes of the moments (Dy^{3+}: 10 μ_B; Yb^{3+}: 1.15 μ_B [7]), we estimate that the dipole interaction in $Yb_2Ti_2O_7$ amounts to only a few per cent of the total interaction. This is necessarily an approximate value (the orientations of the moments are not the same for Dy^{3+} and Yb^{3+}), but it is sufficiently small to indicate that the dominant contribution to the inter-ionic interaction in $Yb_2Ti_2O_7$ is the exchange.

Susceptibility and magnetization measurements were also made on a single crystal with the aim of examining whether any information could be obtained concerning a possibly anisotropy in the Yb^{3+}–Yb^{3+} inter-ionic coupling. The sample was shaped in the form of a flat disc with the principal directions [100], [111] and [011] lying in the plane of the disc and the applied field was applied in turn along these three directions.

In principle, any anisotropy in the coupling could be evidenced either by examining whether the field and temperature dependence of the magnetization shows an angular dependence which differs from that due to the anisotropy of the g-tensor or by examining whether the Curie–Weiss temperature obtained from the susceptibility shows an angular dependence. In the present case, however, it is difficult to carry out an anisotropy analysis because the influence of any anisotropy is attenuated by the presence of the four inequivalently oriented sites. This is illustrated by the behaviour of the anisotropy associated with the g-tensor: the calculated maximum anisotropy in the saturated magnetic moment for the sample after averaging over the four differently oriented sites amounts only to 4%. A further complicating feature for the magnetization measurements is that both the anisotropy in the inter-ionic coupling and the anisotropy of the g-tensor will contribute to the total anisotropy and these two anisotropies may not have the same principal axes.

The net result of the analysis of the single-crystal data is, first, that the results obtained are compatible with those given above for the polycrystalline sample and, second, that although no clear evidence was obtained to show that the inter-ionic exchange is anisotropic, we cannot rule out an anisotropy amounting to as much as a few tens per cent.

3.3. ^{172}Yb perturbed angular correlation (PAC) measurements and the crystal-field analysis

The PAC technique provides the thermal dependence of the quadrupole hyperfine interaction at the ^{172}Yb nucleus. For the D_{3d} point symmetry of the rare-earth site in the pyrochlore lattice, the quadrupole hyperfine interaction only involves the principal component of the total electric

field gradient (EFG). This is made up of two parts, one which is temperature dependent arising from the 4f shell electrons ($V_{zz}^{4f}(T)$) and one which is essentially temperature independent arising from the lattice charges (V_{zz}^{latt}):

$$V_{zz}(T) = V_{zz}^{4f}(T) + V_{zz}^{latt}. \tag{9}$$

Each of the four Kramers doublets fashioned by the crystal field has a different wave function and energy and each adds a different 4f shell contribution to the total EFG at the nucleus. The thermal dependence of the EFG thus reflects the size and sign of the contributions coming from the different crystal-field levels and their Boltzmann populations. In the limit of very high temperatures, when all the crystal-field levels are equally populated, only the lattice charges contribute to the EFG. The CEF analysis method is thus based on the measurement of the total EFG over an extended temperature range (up to 1087 K) and on the derivation of a set of crystal-field parameters which reproduces the experimental variation. The set of CEF parameters is also constrained to reproduce the g-values of the ground doublet reported in section 3.1.

For the PAC measurements, about 100 mg of $Yb_2Ti_2O_7$ was first proton activated to produce radioactive ^{172}Lu and then annealed in vacuum at 800 °C for 24 hours to remove the defects introduced by the irradiation. We used the 91–1094 keV γ–γ cascade from the $^{172}\text{Lu} \rightarrow {}^{172}\text{Yb}$ β-decay. The cascade has a relatively large anisotropy coefficient $A_2 = +0.28$ and reasonable line intensities of 7% and 97%. The intermediate level of the cascade, namely the 1172 keV excited state of ^{172}Yb, has a spin $I = 3$ and a half-life $T_{1/2} = 8.3$ ns, allowing a perturbation in directional correlations to be observed up to about 40 ns. The measurements were made over the range 50 to 1087 K. Two examples of the PAC spectra are shown in figure 4. The perturbation factor $R(t)$ is determined by the characteristics of the intermediate nuclear state in the cascade and by the associated hyperfine interaction [10]. Spectra measured below about 100 K are influenced by dynamical phenomena most probably linked to the paramagnetic relaxation of the Yb^{3+} moments. When the temperature is increased above 100 K, the relaxation rate is sufficiently high that only a static quadrupole interaction is observed. All of these spectra can be well described by assuming a perturbation factor due to a unique, static electric quadrupole hyperfine interaction within an intermediate state with spin $I = 3$. As the local symmetry is axial, the asymmetry parameter of the EFG (η) was fixed at zero. Above 400 K, where the spectra have higher frequencies, the symmetry can be checked experimentally and, when η is fitted, it is found to be zero within experimental error. In order to calculate the z-component of the EFG tensor V_{ij} from the fitted hyperfine frequency: $\nu_Q = |eQV_{zz}/h|$, we used a value $Q(^{172}\text{Yb}, 1172\ \text{keV}) = -3.10$ b for the quadrupole moment [11]. The EFG obtained at the different temperatures is shown by the open points in figure 5. The full data point at 4.2 K was obtained by scaling to ^{172}Yb the value obtained by ^{170}Yb Mössbauer spectroscopy for $(Y_{0.99}Yb_{0.01})_2Ti_2O_7$ (section 3.1) where the relevant quadrupole moment has the value $Q(^{170}\text{Yb}, 84\ \text{keV}) = -2.14$ b [12]. The Mössbauer measurement was also used to determine the sign of V_{zz} at 4.2 K (only the absolute value of V_{zz} can be derived from the PAC spectra for a γ–γ cascade) and this turns out to be positive. As shown in figure 5, when the temperature increases, V_{zz} passes through a zero value meaning that it changes sign to become negative above about 200 K. The negative sign of the high-temperature asymptotic value (where the gradient is dominated by the lattice contribution) is also consistent with the sign found by scaling the lattice contribution observed for Gd^{3+} in $Gd_2Ti_2O_7$ (see below).

We fitted the measured thermal dependence of V_{zz} using the Hamiltonian (1), with the six allowed B_n^m-coefficients and V_{zz}^{latt} as free parameters starting from the set of 'unpublished' crystal-field parameters cited in reference [3]. We obtain the very good fit shown as a solid

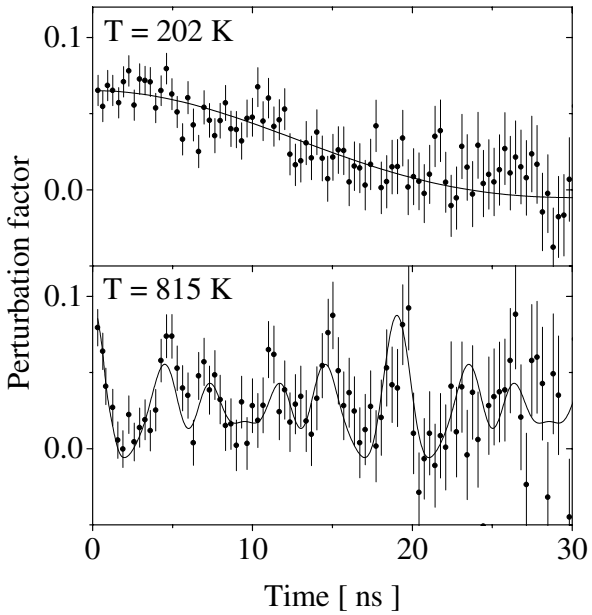

Figure 4. ^{172}Yb perturbed angular correlation spectra of $Yb_2Ti_2O_7$. The solid lines show the fitted perturbation factor due to an electric quadrupolar interaction for $I = 3$. The decrease in the period of the oscillation with increasing temperature evidences an increase in the quadrupolar frequency.

line in figure 5 with the following CEF parameter values:

$$\begin{aligned} B_2^0 &= 12.4\ \text{K} \qquad B_4^0 = -0.178\ \text{K} \qquad B_4^3 = -6.8\ \text{K} \\ B_6^0 &= 0.021\ \text{K} \qquad B_6^3 = -0.14\ \text{K} \qquad B_6^6 = 0.161\ \text{K} \end{aligned} \tag{10}$$

and $V_{zz}^{latt} = -223\ \text{V Å}^{-2}$. This lattice component compares reasonably well with that obtained from ^{155}Gd Mössbauer spectroscopy measurements at 4.2 K for $Gd_2Ti_2O_7$ ($-252\ \text{V Å}^{-2}$) [13] where the measured value is $eQV_{zz} = -792$ MHz and the ground-state quadrupole moment 1.30 b [14]. Because Gd^{3+} is an S-state ion, only the lattice charges contribute to the EFG.

The Yb^{3+} CEF scheme corresponds to four Kramers doublets with energies 0, 620, 740 and 950 K and to a ground-doublet wave function:

$$|\psi_g\rangle = 0.889|J_z = \pm 1/2\rangle - 0.242|J_z = \mp 5/2\rangle + 0.388|J_z = \pm 7/2\rangle \tag{11}$$

for which $g_z = 1.77$ and $g_\perp = 4.18$, close to experimental findings.

Some sets of crystal-field parameters for Yb^{3+} in the pyrochlore lattice have been published [15–18]. All are inappropriate as each corresponds to a crystal level scheme and to a ground-state wave function which are not compatible with the experimental data presented here. A much more relevant 'unpublished' set of crystal-field parameters is cited in reference [3]. This set gives a ground-state wave function with a g-tensor which has the correct anisotropy and approximately the correct size but leads to a calculated thermal variation of the 4f shell quadrupole hyperfine interaction which is stronger than that observed experimentally. Recently a set of crystal-field parameters based on inelastic neutron scattering measurements has been proposed for Ho^{3+} in $Ho_2Ti_2O_7$ [19]. When used for Yb^{3+}, this set predicts a ground state which is a well isolated Kramers doublet with a g-tensor which has the correct anisotropy and approximately the correct size. The calculated thermal variation of the 4f shell quadrupole moment is however slightly stronger than observed experimentally. Conversely, when our

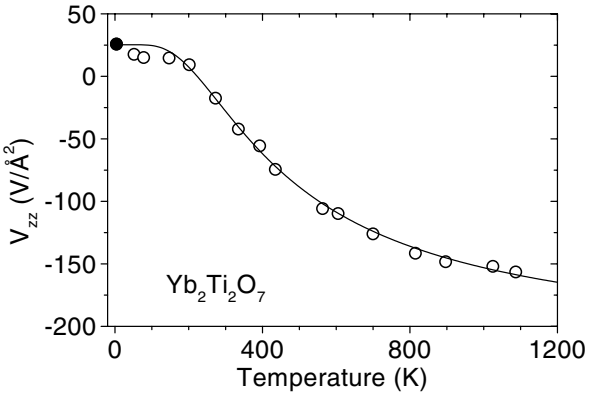

Figure 5. The thermal dependence of the electric field gradient in $Yb_2Ti_2O_7$ obtained from ^{172}Yb perturbed angular correlation measurements (open points). The full point at 4.2 K was obtained from a ^{170}Yb Mössbauer measurement. The solid line was calculated using the set of crystal-field parameters given in the text.

Yb^{3+} CEF parameters are used to calculate the CEF properties for Ho^{3+} in $Ho_2Ti_2O_7$, they give a ground-state doublet mainly composed of $|M_J = 8\rangle$ and $|M_J = -8\rangle$, as found in reference [19], but there are differences for the excited levels. The difference between the CEF parameters for Yb^{3+} and Ho^{3+} may, in part, result from the presence of a slight variation of the CEF parameters across the rare-earth series: structural studies [9] have shown that both the free parameter (x) which governs the positions of the close oxygen neighbours and the lattice parameter change slightly as a function of the rare earth.

4. Summary

The present study was motivated by the need to obtain detailed information concerning the Yb^{3+} crystal field and the inter-ionic interactions in $Yb_2Ti_2O_7$. Such information is a prerequisite to any understanding of the low-temperature magnetic properties and of the role of geometrically derived magnetic frustration.

We have obtained a set of crystal-field parameters which accounts for all the currently known CEF-based data: $B_2^0 = 12.4$, $B_4^0 = -0.178$ K, $B_4^3 = -6.8$ K, $B_6^0 = 0.021$ K, $B_6^3 = -0.14$ K, $B_6^6 = 0.161$ K. A more refined set could be obtained by incorporating the results of future neutron inelastic scattering measurements. We find that the Yb^{3+}-ion ground state is a well isolated Kramers doublet having a planar anisotropy ($g_\perp/g_\parallel = 2.4$). The three exited Kramers doublets lie at 620, 740 and 940 K. The Yb^{3+}–Yb^{3+} coupling, which is ferromagnetic, is dominated by the exchange interaction, and it has an average strength of 0.3 T/μ_B. This coupling may be anisotropic.

Under the influence of the frustration, the low-temperature magnetic properties of $Yb_2Ti_2O_7$ are unusual. They are described elsewhere [7] and are summarized as follows. There is no long-range magnetic order at temperatures below that of the known specific heat λ-transition ($\sim$0.2 K) [2]. As the temperature is lowered through $\sim$0.2 K there is a first-order reduction, by a factor of 10^2–10^4, in the fluctuation rate of the short-range-correlated Yb^{3+} moments and, below 0.2 K, these moments continue to fluctuate at a temperature-independent rate.

References

[1] Subramanian M A, Aravamudan G and Subba Rao G V 1983 *Prog. Solid State Chem.* **15** 55
[2] Blöte H W J, Wielinga R F and Huiskamp W J 1969 *Physica* **43** 549
[3] Greedan J E 1992 *Landolt–Börnstein New Series* Group III, vol 27g (Berlin: Springer) pp 87–123
[4] Harris M J, Bramwell S T, McMorrow D F, Zeiske T and Godfrey K W 1997 *Phys. Rev. Lett.* **79** 2554
[5] Ramirez A P, Hayashi A, Cava R J, Siddharthan R and Shastry B S 1999 *Nature* **399** 333
[6] den Hertog B C and Gingras M J P 2000 *Phys. Rev. Lett.* **84** 3430
[7] Hodges J A *et al* 2001 submitted
[8] Bramwell S T, Field M N, Harris M J and Parkin I P 2000 *J. Phys.: Condens. Matter* **12** 483
[9] Knop O, Brisse F and Castelliz L 1969 *Can. J. Chem.* **47** 971
[10] Frauenfelder H and Steffen R M 1968 *Alpha-, Beta-, Gamma-Ray Spectroscopy* ed K Siegbahn (Amsterdam: North-Holland) ch 19A
[11] Królas K and Rams M 1996 *Hyperfine Interact.* C **1** 159
[12] Raghavan P 1989 *At. Data Nucl. Data Tables* **42** 189
[13] Armon H, Bauminger E R and Ofer S 1973 *Phys. Lett.* B **43** 380
[14] Tanaka Y, Laubacher D B, Steffen R M, Shera E B, Wohlfahrt H D and Hoehn M V 1982 *Phys. Lett.* B **108** 8
[15] Townsend M G and Crossley W A 1968 *J. Phys. Chem. Solids* **29** 593
[16] Dunlap B D, Shenoy G K, Friedt J M, Meyer M and McCarthy G J 1978 *Phys. Rev.* B **18** 1936
[17] Sonderholm L, Stager C V and Greedan J E 1982 *J. Solid State Chem.* **43** 175
[18] Sengupta A, Jana J and Ghosh D 1999 *J. Phys. Chem. Solids* **60** 331
[19] Rosenkranz S, Ramirez A P, Hayashi A, Cava R J, Siddharthan R and Shastry B S 2000 *J. Appl. Phys.* **87** 5914
[20] Dattagupta S 1984 *Hyperfine Interact.* **11** 77
[21] Bramwell S T, Gingras M J P and Reimers J N 1994 *J. Appl. Phys.* **75** 5525